Separation and Purification Technology 278 (2022) 119106

Contents lists available at ScienceDirect

Separation and Purification Technology

journal homepage: www.elsevier.com/locate/seppur

Adsorptive removal of fluoride using biochar – A potential application in drinking water treatment

Mohini Sadhu [a], Prosun Bhattacharya [b,c], Meththika Vithanage [d,e,f], Pamidimukkala Padmaja Sudhakar [a,*]

[a] Department of Chemistry, Faculty of Science, The M.S. University of Baroda, Sayajigunj, Vadodara 390002, India
[b] KTH-International Groundwater Arsenic Research Group, Department of Sustainable Development, Environmental Science and Engineering, KTH Royal Institute of Technology, Teknikringen 10B, SE-10044 Stockholm, Sweden
[c] KWR Watercycle Research Institute, Groningenhaven 7, 3433 PE Nieuwegein, The Netherlands
[d] Ecosphere Resilience Research Center, Faculty of Applied Sciences, University of Sri Jayewardenepura, Nugegoda 10250, Sri Lanka
[e] Instrument Center, Faculty of Applied Sciences, University of Sri Jayewardenepura, Sri Lanka
[f] Molecular Microbiology and Human Diseases, National Institute of Fundamental Studies, Kandy 20000, Sri Lanka

ARTICLE INFO

Keywords:
Watermelon rind biochar
Fluoride
Adsorption
Groundwater
Industrial wastewater

ABSTRACT

Fluoride as a geogenic contaminant is commonly encountered in groundwater-based drinking water sources. In the present study Watermelon Rind (*Citrullus lanatus*) Biochar (WMRBC) was investigated for its defluoridation potential. The factors affecting the removal of fluoride, including pH, adsorbent dosage, initial concentration, and contact time were investigated. The experimental data were fitted well by Freundlich isotherm and pseudo-second-order model, the maximum fluoride adsorption capacity being 9.5 mg/g. Thermodynamic parameters indicated that the fluoride adsorption process was a spontaneous exothermic process. The presence of other anions like HCO_3^-, CO_3^{2-}, Cl^-, SO_4^{2-}, and NO_3^- (100 mg/L) had little effect on the adsorption of fluoride at 50 mg/L. Characterization studies of WMRBC before and after fluoride adsorption by SEM, ATR, EDX and XRD techniques, indicated that the adsorption of fluoride may be by electrostatic attraction through protonated basic functionalities present in WMRBC and by precipitation at the mineral sites. WMRBC could be a viable adsorbent for effective removal of fluoride from drinking water and industrial wastewater.

1. Introduction

Groundwater is the most abundant and readily available source of global freshwater supply and will continue to be the most valuable resource over several decades to come [1,2]. Fluoride is an important globally recognized contaminant in drinking water [3]. Fluoride occurs in the environment due to the presence of fluoride-containing minerals , viz., fluorite, biotite, topaz, etc., in the earth's crust as well as from industrial activities, specially semiconductor, electroplating, glass, steel, cement, aluminium smelter ceramic and fertilizers industries [4]. The discharge of wastewaters from these industries as well as run-off leads to fluoride contamination of surface and groundwater. The hydrology of groundwater in hydrogeological environments will thus be dependent on the physicochemical properties of ground water, industries and fluoride mineral containing rocks [5]. It is well known that chronic exposure to fluoride through drinking water leads to an increased risk of dental and bone fluorosis in a dose-responsive manner [6,7].

Groundwater fluoride levels above WHO limits (0.5 and 1.0 mg/L) has emerged as a global problem especially in arid and semi-arid regions [8]. Groundwater is the major source of drinking water in the rural areas of developing countries like India, China and parts of Africa [5,6,9,10]. Fluoride contamination in ground water is reported to have socio-economic developmental implications due to abandonment of the contaminated drinking water sources such as bore wells while chronic consumption of such fluoride contaminated water has resulted in fluorosis among many people [11].

Some of the conventional methods such as precipitation [12], ion-exchange [13,14], adsorption [15,16], reverse osmosis [17], nano-filtration [18], donnan dialysis [19], electrodialysis [18,20] and electrochemical technologies, including electrocoagulation [20], electroflotation and electrochemical oxidation [21], have been proposed for removal of fluoride from wastewater and drinking water samples.

* Corresponding author.
E-mail address: p_padmaja2001@yahoo.com (P. Padmaja Sudhakar).

https://doi.org/10.1016/j.seppur.2021.119106
Received 6 February 2021; Received in revised form 1 June 2021; Accepted 5 June 2021
Available online 9 June 2021

Among these methods, adsorption has been widely used as a cost effective, and highly efficient technique towards fluoride removal [21–23].

Biochar generally produced by biomass pyrolysis has been heralded as a cost effective adsorbent [24,25]. Previous studies showed that pyrolysis conditions, particularly the pyrolysis temperature significantly affected the elemental composition, chemical structure, and stability of biochar [26].

The characteristics of raw feedstock biomass such as ash content, its elemental constituents, density, and hardness impart specific properties to the resulting biochar [27,28]. Biochar has been used for removal of herbicides [29,30], pesticides [31] and fungicides [32].

Very little work has been done on the use of biochar for the removal of fluoride .Magnetic and nonmagnetic biochars from corn stovers [26] as well as pine wood and pine bark chars [33] were used by Mohan et al. for the removal of fluoride at pH 2. Nano sized rice husk biochar [34] has been fabricated by Goswami et al. for removal of F^-. However, in these studies, they have applied the biochar for removal of fluoride from ground water. The adsorbents used so far for industrial wastewater are bio adsorbents such as banana peel, groundnut shell and perennial grass [35,36].

Citrullus lanatus (Watermelon) is a fruit of great economic importance, belonging to Cucurbitaceae family. Its worldwide production was estimated to be approximately 93,700 million tons [37].Watermelon Rind (WMR) is utilized in products such as pickles and preserves as well as for extraction of pectin while watermelon seeds are a potential source of protein [38].The rind is one of the major solid wastes generated by several restaurants, and cottage food industries in India.

WMR is fairly rich in carbohydrates, phenolic compounds and fatty acids. The carbohydrate fraction of melon rind is mainly composed of cellulose, hemicelluloses and pectin, comprising glucose, xylose and galactose as the major monosaccharides, causing WMR to be a potential candidate for biochar fabrication [39–41].

The main objective of this work was to evaluate the defluoridation potential of WMR derived biochar (WMRBC) produced by pyrolysis at 400 ^{0}C (at the rate of 10 °C/minute) for 4 h from aqueous solutions. The temperature, rate of pyrolysis and residence time were based on preliminary optimisation studies that gave a maximum yield of 30.8% The physicochemical characteristics of WMRBC were determined and its defluoridation efficiency was optimised by batch adsorption as a function of pH, contact time, adsorbent dose and temperature. The performance of the biochar was evaluated as a function of Langmuir, Freundlich, Temkin and Halsey adsorption models. Further, the adsorption thermodynamics and kinetics were investigated to get an insight into the adsorption mechanism. The adsorption capacity of WMRBC was compared with literature reported adsorbents for removal of fluoride for future application for defluoridation of real water systems.

2. Materials and methods

2.1. Synthesis and characterisation of watermelon rind biochar (WMRBC)

Dried WMR were collected from the local fruit shop of Vadodara, Gujarat, India, washed, dried in an oven at 100 °C for 24 h and then ground to fine powder. The ground powder was sieved through 18 mesh size sieve and stored in airtight container. The sieved powder was pyrolysed at 400 ^{0}C (at the rate of 10 °C/minute) for 4 h in muffle furnace. The resultant biochar was washed with hot water and finally it was dried in oven at 100 °C (WMRBC).

The surface functional groups in WMRBC before and after adsorption of fluoride were investigated by Attenuated Total Reflection Fourier Transform Infrared (ATR-FTIR) spectroscopy (model NicoletTM iS50, make Thermofisher). Thermogravimetric analysis (TGA) of WMRBC was performed using EXSTAR6000 TG/DTA 6300 model under nitrogen atmosphere. Samples weighing about 2.5 mg were taken in the sample pan and the temperature was raised from 30 to 700 °C at a heating rate of 10 °C per minute. The mass of the sample pan was continuously recorded as a function of temperature.

Scanning Electron Microscopy (SEM) was performed on JEOL 1600 to observe the surface morphology of pristine WMRBC and WMRBC after adsorption of fluoride (WMRBCF). A dried sample was placed on metal stub with adhesive and coated with gold using a JEOL auto fine coater. The accelerating voltage was −10–20 keV. The Brunauer-Emmett-Teller (BET) surface area was determined by nitrogen gas adsorption at 77.3 K by using computer-controlled BET surface area and porosity analyser (make: Micromeritics, model: ASAP 2020).

Energy Dispersive X-ray Analysis (EDAX) technique was used for performing elemental analysis in conjunction with Scanning Electron Microscopy (SEM). The intensity or area of a peak in an EDAX spectrum is proportional to the concentration of the corresponding element in the specimen. The elemental content was determined by assuming that the electron-beam current was uniform throughout the specimen and electron channelling was avoided by tilting the specimen away from any main zone-axis which prevents strong diffraction conditions.

XRD measurements of the powder samples were performed with a PANalytical X-Ray Diffractometer (Bruker) with Cu-Kα radiation (λ = 0.15418 nm) at a voltage of 45 kV and with a scanning range of 2 theta 0°-90° with a scan time of 0.2 s at a increment of 0.05°.

The point of zero charge (PZC) and the zeta potential of WMRBC at different pH was measured using Zeta Plus 90Plus/BI-MAS Brook Haven model Zeta sizer.

2.2. Fluoride uptake studies

Stock solutions of fluoride were prepared by dissolving 2.2105 g sodium fluoride (Spectrochem) in 1000 mL of conductivity water followed by dilution to the desired concentration.

The fluoride uptake studies were conducted in batch mode by taking known weight of WMRBC dispersed in 100 mL polypropylene flask containing fluoride in the concentration range 1–100 mg/L. The flasks were shaken orbitally at a constant rate of 150 rpm for 3 h at room temperature (35 ± 2 °C in the month of June). The adsorbent after fluoride uptake was separated by filtration and dried for further analysis. The fluoride remaining unadsorbed in the solution was measured by fluoride ion selective electrode (Thermo scientific ORION STAR A214) after preparing a calibration graph by analysing known concentrations of fluoride solutions. During the analysis TISAB IV (supplied by Metroohm was used. Briefly, 58 g NaCl was dissolved in approximately. 500 mL deionised·H_2O, 5 g complexon IV was added and dissolved by drop wise addition of 8 mol/L NaOH. This was followed by the addition of 57 mL glacial acetic acid and adjustment of the pH of the mixture to 5.5 with the above mentioned NaOH solution. Finally it was made up to 1 L with deionised·H_2O) buffer of about 15 mL/ 50 mL of the fluoride containing solution was added to maintain the pH 5–7. The amount of fluoride uptake was calculated using the formula:

$$q_e = C_i - C_e/m^*100 \quad (1)$$

where q_e is the fluoride uptake (mg/g), C_i is initial fluoride concentration (mg/L), C_e is equilibrium fluoride concentration (mg/L), V is volume of solution (L) and m is mass of the adsorbent (mg).

All experiments, except pH variation studies, were conducted at pH 1.

The experimental data were fitted to several isotherm and kinetic models (Table S1) to understand the adsorption process. The regenerability, reuse and applicability of WMRBC in defluoridation of industrial effluents and ground water samples was further investigated.

3. Results and discussion

3.1. Characterisation of WMRBC

3.1.1. XRD analysis

The XRD spectrum of WMR (Fig. 1) shows predominantly the peaks characteristic of cellulose. The broad peak around 22.8 can be indexed to carbon (0 0 2) diffraction plane while the weak broad peak at 2θ of 44 corresponds to the graphitic (1 0 0) crystalline lattice of turbostratic carbon (i.e. very little or no stacking order between small graphene planes) in WMRBC and WMRBCF. These small graphene planes arranged in turbostratic disorder were observed by several other researchers [42,43]. Further, other sharp peaks observed at 28.5 and 40.6 were attributed to mineral crystals in the biochar such as quartz (q) and sylvite (s). The K in biochars is mostly present in the form of KCl (sylvite), K_2SO_4 and K_2CO_3, whereas P mostly exists as $Ca_2P_2O_7$ [44].The peak at 30.7 indicated the calcite (c) ($CaCO_3$) content of biochar but in addition, exhibited XRD peaks for the mineral whitlockite (w). The presence of whitlockite (beta-tricalcium phosphate), which can also have Mg in the structure, is consistent with P, Ca and Mg content in EDAX [45]. The average crystallite size calculated by Scherrer equation was ~ 38 nm.

3.1.2. Thermogravimetric analysis

Figure S1 shows the thermogram of WMRBC adsorbent. The first stage weight loss (~20%) from 50°-100 °C was attributed to loss of water, indicating that the sample contains very less moisture. At 265 °C to 500 °C, the mass of biochar decreased by 85% due to the vaporization of volatile matter and degradation of cellulose, hemicellulose and lignin components. The large weight loss suggested higher volatile matter content in the biochar. Hemicellulose is reported to thermally decompose at 250 °C and continue up to 380 °C, cellulose degradation occurs between 300 °C and 400 °C while lignin degradation takes place at 200–500 °C [46]. Since there was no significant weight loss from 500 to 700 C, the 11% residue indicated the fixed carbon content along with minerals such as quartz, calcite, sylvite and whitlockite as identified by XRD.

3.1.3. Scanning electron microscopy and energy dispersive X-ray analysis

The surface of pristine WMR (Fig. 2) appeared to be less porous than the surface of WMRBC. The surface of WMRBCF became brighter, with appearance of some deposition on pores indicating the possible deposition of fluoride [47] as metal fluorides such as Ca, Mg and K as evidenced from EDAX analysis.

The insets of Fig. 2 show the EDAX analysis of WMRBC and

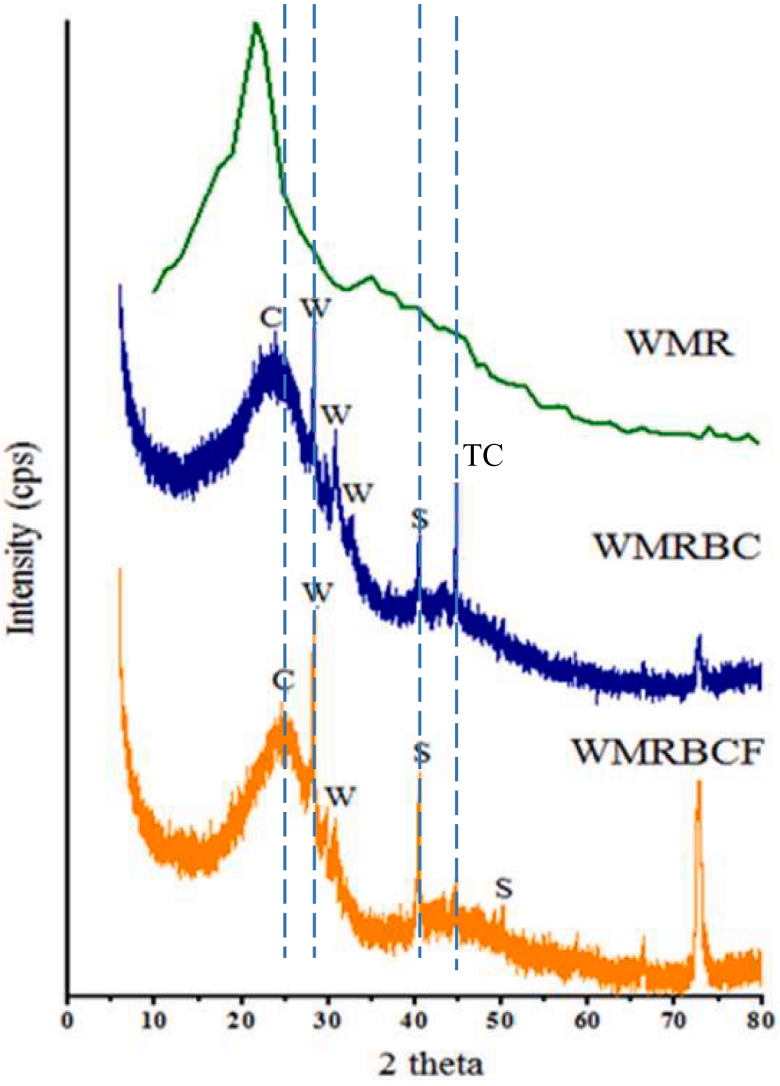

Fig. 1. XRD spectra of WMR, WMRBC before and after fluoride adsorption (WMRBCF).

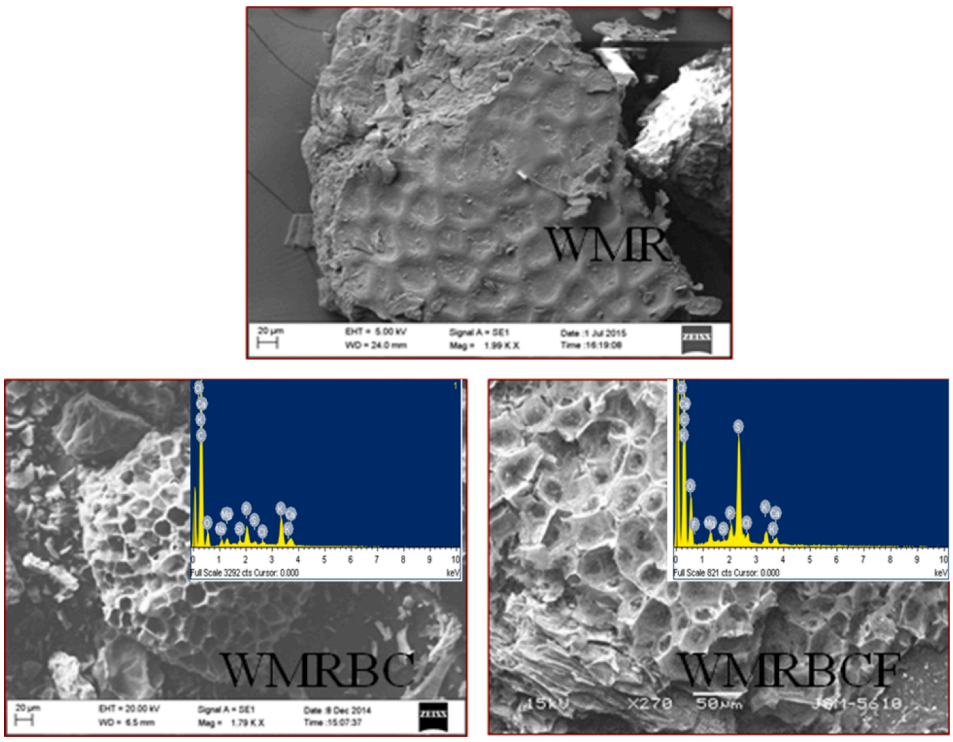

Fig. 2. SEM images of WMR, WMRBC before and after adsorption with insets depicting EDS spectra of WMRBC before and after adsorption.

WMRBCF. Appearance of fluoride peak in EDAX Spectra of WMRBCF indicated successful adsorption of fluoride. Substantial increase in S and O content in WMRBCF could be due to uptake of sulphate ions present in water along with fluoride on agitation for 3 h at pH 1. EDAX studies after fluoride adsorption further indicated that there was no significant change in Ca content. The organic acid component of the biochar may have contributed to complexation of Ca and Mg. There was only a decrease in K content.

The results of the XRD analysis, together with the FITR spectra and EDAX analysis, demonstrated the existence of carbonate and phosphate-rich species as the main constituents of the inorganic fraction of the biochar samples.

3.1.4. ATR-FTIR spectral analysis

The IR spectral analysis of WMR, WMRBC and WMRBCF was performed and corresponding spectra are presented in Fig. 3. The FTIR spectra of WMR exhibited characteristic absorption bands corresponding to celluloses and hemicelluloses of polysaccharides (1000–1200 cm^{-1}) and broad O═H stretching of hydroxyl groups at 3200–3400 cm^{-1}. The C-H stretching vibrations of aliphatic groups was observed in the range 2980–2820 cm^{-1} [48].The absorption bands at 1610–1740 cm^{-1}, corresponded to C═O stretching of ketones and other carbonyl structures of WMR. The band observed at 1030

cm^{1}, was attributed to C—O and C—O—C stretching, characteristic of the anomeric region of cellulose-like structure, while the band at 1590 cm^{-1} was attributed to aromatic C═O and C═C stretching and the bands observed at 700–850 cm^{-1} were assigned to aryl C—H and/or aryl C—O groups. At low pyrolysis temperature (360 °C), the biochars were reported to behave like the feedstock maintaining a certain hydration and a carbohydrate structure, due to the partial chemical conversions occurring at these conditions [49].

The characteristic absorption bands of cellulose and hemicellulose polysaccharides (1000–1200 cm^{-1}) were of reduced intensity in WMRBC. Pyrolysis has also resulted in negligible O-H stretching of the hydroxyl groups at 3200–3400 cm^{-1}, due to the loss of hydration, as well as weak C-H stretching of the aliphatic groups (2980–2820 cm^{-1}). This could be attributed to reduction in unstable aliphatic compounds caused by the demethoxylation, demethylation, and dehydration of lignin during the preparation of biochar [50]. The bands due to C-H stretching vibrations of methyl and methylene groups observed at 2984 cm^{-1} and 2894 cm^{-1} respectively in pristine WMRBC have been shifted to 2981 and 2896 cm^{-1} after fluoride adsorption, along with the appearance of a new peak at 997 cm^{-1} indicative of C—F stretching [51].

However the absorption intensities at 1610–1740 cm^{-1}, corresponding to C═O stretching of ketones and other carbonyl structures [49] of pristine WMR could be reasonably retained in the biochar. Even the band at 1030 cm^{-1}, corresponding to C—O and C—O—C stretching, characteristic of the anomeric region of cellulose-like structure [52] was visible with reasonable intensity in the biochar. Intensity of the peaks corresponding to aromatic C═O and C═C stretching at 1590 cm^{-1} also slightly increased with pyrolysis as well as the peak at 700–850 cm^{-1} corresponding to aryl C-H and/or aryl C-O groups. Pyrolysis, further resulted in removal of carboxylic and carbonyl groups (1700 cm^{-1}), suggesting that they could be due to inorganic carbonates [53].

3.1.5. Physicochemical analysis of WMRBC

The physicochemical properties of WMRBC which include density, pH value, moisture content, Brunauer–Emmett–Teller surface area (BET), ion exchange capacity and iodine sorption values were investigated [51]. The values are listed in Table 1. The pH was measured by taking 1 g of adsorbent in 100 mL distilled water and heated to boiling with constant stirring for 30 min. For measuring moisture content, a known weight of sample was heated in air oven maintained at 105 ± 5 °C for about 3 h .The procedure was repeated till constant weight was obtained. For bulk density measurements, a previously weighed 100 mL graduated cylinder was filled up to 50 mL mark with WMRBC without tapping. The cylinder with the biochar was weighed accurately. The bulk density was calculated by dividing the difference in weight of the cylinder with biochar and without biochar by 50. To measure the ion exchange capacity, 0.5 g of WMRBC was added to 100 mL of 0.25 M sodium sulphate in a stoppered conical flask and kept for shaking in a

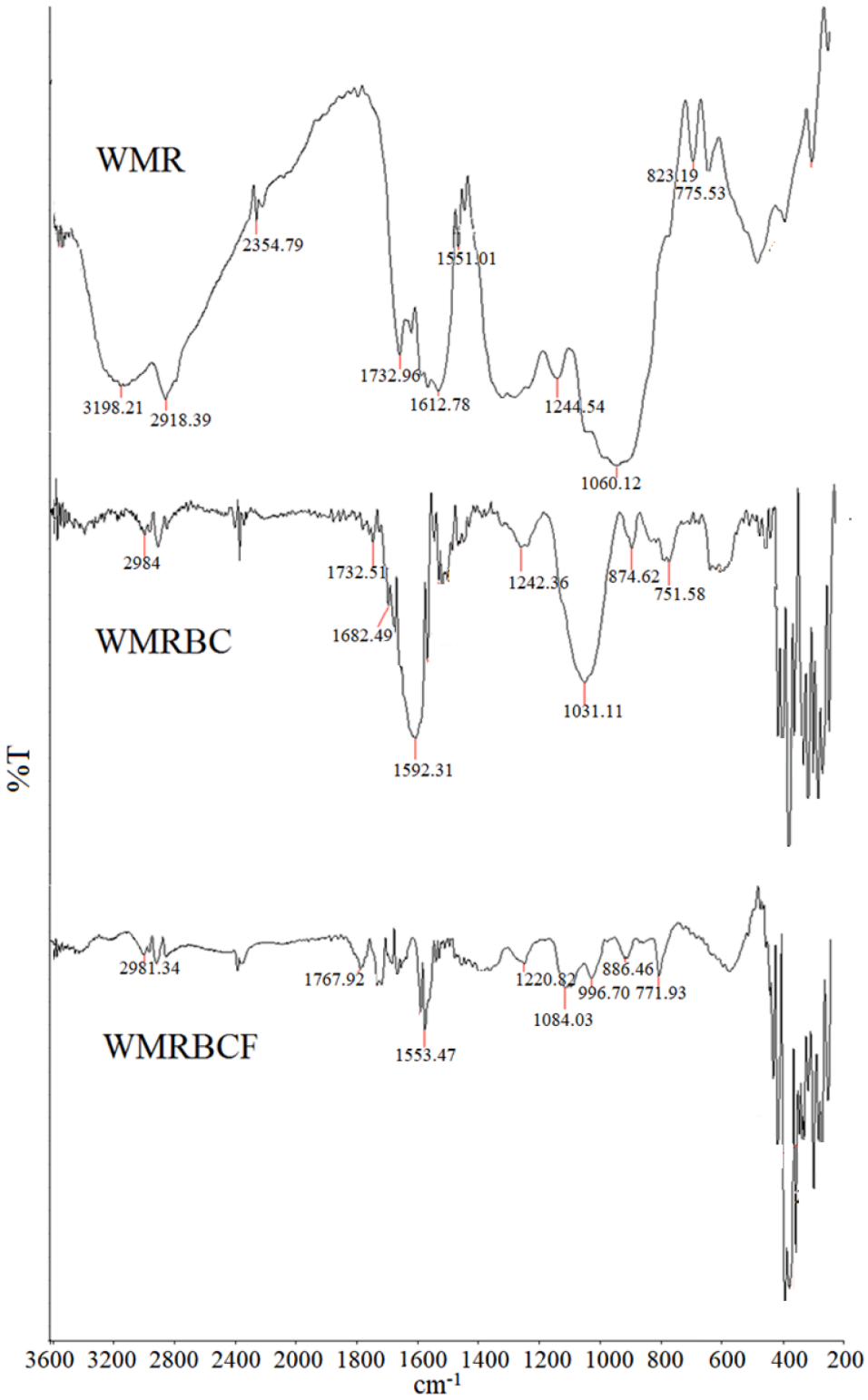

Fig. 3. IR spectra of WMR, WMRBC and WMRBC after fluoride adsorption (WMRBCF).

temperature-controlled bath. After 5 h, the contents were filtered and the filtrate was titrated against 0.1 N NaOH using phenolphthalein. The ion exchange capacity of the adsorbent in meq/g was calculated from the equation:

$$\text{Ion exchange capacity}\left(\frac{\text{meq}}{\text{g}}\right) = \frac{\text{aW}}{\text{V}} \quad (2)$$

Where, a = Normality of NaOH

V = Volume of NaOH

W = Weight of the adsorbent in g

Iodine value was measured by means of adsorption of iodine from aqueous solution. It is used to compare adsorbent surface areas and is a relative indicator of porosity [52]. About 0.2 g of WMRBC was equilibrated with iodine solution. The residual iodine concentration was determined by titrating with sodium thiosulphate solution.

Table 1
Physico-Chemical properties of WMRBC.

Parameters	Value
pH	9.2
Moisture content	10.3927%
Bulk density	0.4921 g/mL
Cation exchange capacity	0.033 meq/g
Iodine value	389.93 mg/g
BET surface area	0.5365 m^2/g

Iodine value= (Blank-Burette reading for sample) × Conversion factor; mg/g (3)

$$\text{Conversion factor} = \frac{\text{Mol. Wt. of Iodine } (127) \times 40}{\text{Wt. of Carbon} \times \text{Blank Reading}} \quad (4)$$

Where, blank reading is the burette reading for iodine concentration without addition of adsorbent and burette reading is for iodine remaining un-adsorbed in solution after adding biochar.

The porosity of the WMRBC was determined by BET surface area analyser at 77.3 K. The specific surface area was calculated from the isotherm using the BET equation:

$$\frac{1}{v\left[\left(\frac{P_0}{P}\right)\right] - 1} = \frac{C-1}{v_m C}\left(\frac{P}{P_0}\right) + \frac{1}{v_m C} \quad (5)$$

P and P_0 are the equilibrium and the saturation pressure of adsorbate at the adsorption temperature, v is the adsorbed gas quantity (in volume units), and v_m is the volume of gas adsorbed in a monolayer, c is the BET constant, which is expressed by:

$$c = \exp\left(\frac{E_1 - E_L}{RT}\right) \quad (6)$$

The biochar could adsorb nonpolar iodine molecules and had a cation exchange capacity of 0.033 meq/g.

3.2. Fluoride uptake studies

3.2.1. Effect of pH

The effect of pH on adsorption of fluoride onto 0.1 g of WMRBC was investigated in the pH range 1.0–11.0 (Figure S2(a)) at an initial fluoride concentration of 50 mg/L by agitating for 3 h. It was observed that maximum adsorption occurred at pH 1 with a sharp decrease in adsorption efficiency above pH 2

To understand this observation the change in surface charge of the adsorbent was investigated by measuring the zeta potential of WMRBC as a function of pH. It was observed that the zero point charge of WMRBC was observed to be at pH 2.1 above which the surface charge of the adsorbent was observed to be negative (Figure S2(b)).

Higher hydronium ion concentrations at low pH will protonate basic functions in the WMRBC, making them amenable to bind fluoride ions. Similar observations were made by Dinesh et al. during removal of fluoride by pine bark and pine wood [53]. These protonated functionalities can attract hydrated fluoride ions. Further hydrated ion pairs of H_3O^+ F^-can diffuse into the biochar pore walls and F^- can be exchanged to protonated functionalities within the pores as well [54].

As pH is increased, fewer protonated sites would be present and fluoride is not efficiently removed. The decrease in fluoride removal under alkaline conditions may be due to electrostatic repulsion of fluoride ions by negative surface charge on WMRBC [55].

3.2.2. Effect of WMRBC dose

Batch sorption experiments with different doses of WMRBC ranging from 25 mg to 50 mg have been carried out to investigate the effect of WMRBC dose on the removal efficiency of 50 mg/L of fluoride in a volume of 25 mL. It was observed that uptake of fluoride increased with increase in WMRBC dose owing to the increased availability of active sites (Fig. 4a).

3.2.3. Effect of contact time

The effect of contact time was investigated by taking 25 mL of 50 mg/L solution of fluoride at pH 1 and equilibrating with 0.2 g of WMRBC for different time intervals (Fig. 4b). Maximum uptake was observed after equilibrating for 3 h and further remained constant. Significant fraction of fluoride (66%) was removed in the first half hour and then increased slowly until equilibrium was reached. The change in the rate of removal might be due to the fact that initially all adsorbent sites were vacant and the solute concentration gradient was high. Later, the fluoride uptake rate by adsorbent decreased significantly, due to the decrease in the number of adsorption sites as well as fluoride concentration [56].

3.2.4. Effect of temperature

Fig. 4c shows effect of temperature on fluoride uptake. It was observed that uptake gradually decreased with increase in temperature suggesting that the adsorption process was exothermic. The decrease in uptake may be due to increased tendency of the molecules to escape from the adsorbent surface to the solution phase resulting in a decrease in thickness of the boundary layer [57].

3.2.5. Effect of initial concentration of fluoride

Effect of initial fluoride concentration (5 to 100 mg/L) on the adsorption process was investigated and is depicted in Fig. 4d. It was observed that the uptake of fluoride decreased with increasing fluoride concentration due to less availability of active sites [57].

Langmuir, Freundlich, Temkin and Halsey isotherms were further used to model the experimental data [58]. The results of the experimental data fitted to these four models and the sorption parameters are shown in Table 2, Fig. 5. and Fig. S3.

The Freundlich model yielded a better fit [r^2 = 0.9989] than the Langmuir model [r^2 = 0.9479] indicating that the adsorption process was taking place on a heterogeneous surface that varied with surface coverage [58,59]. Further, the value of n calculated from the slope of the plot of Freundlich isotherm suggesting favourable adsorption [59].

The Temkin isotherm [60] is characterized by uniform distribution of binding energies. From the Temkin plot shown in Figure S3, the following values were estimated: $A_T = 0.598$ L/g, $b_T = 0.1016$ indicating a physical adsorption process.

The Halsey adsorption isotherm is suitable for multilayer adsorption [61] and the fitting of the experimental data to this model indicated the heteroporous nature of the adsorbent.

The comparison of adsorption capacity of various adsorbents reported in literature for fluoride removal are summarised in Table 3.

It can be observed that the adsorption capacity of WMRBC was better than literature reported biochars, groundnut shell, manganese oxide coated alum and agricultural waste while Aluminium hydroxide based adsorbents, carbon and sweet lime proved better. However, it becomes difficult to come to a conclusion regarding the efficiency of the adsorbents as the sorption capacities have been reported at different pH, temperatures, adsorbent doses, adsorbate concentration ranges, different particle size of the adsorbents and surface areas. It is further difficult to compare the economic feasibility of the material with literature reported biochars because of the difference in preparation conditions, properties, applications and adsorption capacities. Low temperatures and long residence times are more efficient for soft materials. Low temperatures and low heating rates are more effective for greater recovery of biochar [62,63].

3.2.6. Adsorption kinetics and thermodynamics

To study the adsorption kinetics, pseudo-first-order, pseudo-second-

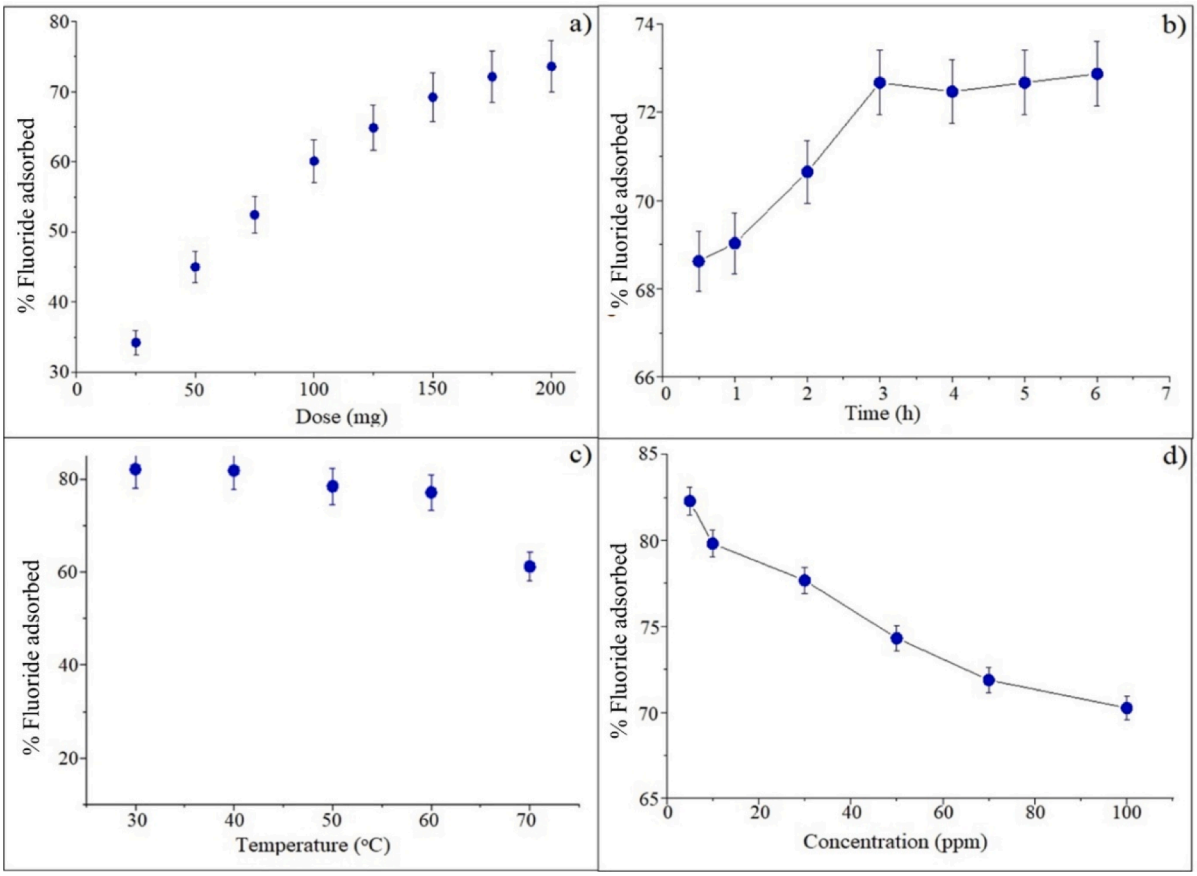

Fig. 4. Effect of a) adsorbent dose b) contact time c) temperature and d) initial concentration of fluoride on % uptake of fluoride (contact time: 3 h for a , c and d; initial fluoride concentration: 50 mg/L for a b and c; pH 1).

Table 2
Isotherm parameters of Langmuir. Freundlich, Temkin and Halsey for the adsorption of fluoride by WMRBC.

	Isotherm Parameters (Q_{exp} 9.5 mg/g)		
Langmuir	Qm	K_L (L.mmol^{-1})	r^2
	17.1823	0.0328	0.9479
Freundlich	N	k_F (L.g^{-1})	r^2
	1.2799	0.6282	0.9989
Temkin	A_T(Lg^{-1})	b_T	r^2
	0.5980	0.1016	0.9754
Halsey	k_H(L.g^{-1})	n_H	r^2
	0.8405	−1.7024	0.9900

order, Elovich and intraparticle diffusion models were investigated (Figures 5 and S4), and the calculated rate constants and r^2 values are given in Table 4.

It was observed that the experimental q_e values were closer to the calculated q_e values of pseudo-second order equation than pseudo-first order equation. The regression coefficient (r^2) value at 303 K was 0.9997 for the pseudo-second order model, suggesting that the pseudo-second order was the best fit kinetic model and that the binding interactions between WMRBC and fluoride were not entirely physical but also included some chemical interactions [64].

Elovich equation is used to describe second order kinetic assuming that the actual solid surfaces are energetically heterogeneous [65]. Higher value of A (46100.35) than B (4.0633) suggested higher adsorption rate than desorption, indicating a viable adsorption process [66].

The study of the intra-particle diffusion model gave r^2 values of 0.9315 and the plot between sorbate concentration and square root of time was linear suggesting that the adsorption process could be controlled by intraparticle diffusion.

The thermodynamic parameters such as change in free energy (ΔG°), enthalpy (ΔH°), and entropy (ΔS°) obtained for the adsorption of fluoride are given in Table 5.

The negative value of enthalpy is due to the exothermic nature of adsorption while the negative value of free energy indicated the feasibility and spontaneous nature of the process. The ΔG° values obtained in this study were more than 20 kJ/mol, indicating that charge sharing or charge transfer was the predominant mechanism in the sorption process [67].

3.2.7. *Effect of competing anions*

Generally, natural water contains several anions. The effect of co-existing anions (e.g. Cl^-, NO_3^-, SO_4^{2-}, HCO_3^- and CO_3^{2-}) on fluoride adsorption by WMRBC was evaluated and is shown in Fig. 6a. Fluoride uptake in the presence of other anions over WMRBC was studied using 8 g/L of WMRBC in 50 mg/L of fluoride solution containing 50 mg/L and 100 mg/L of other anions. The presence of the mentioned anions had negligible effect on fluoride adsorption. The adsorption capacity of WMRBC for 50 mg/L fluoride decreased by ~ 5–7% in the presence of double the concentration of anions under study.

3.2.8. *Application to groundwater sample*

To check the efficiency of the adsorbent, a groundwater sample was collected from Fatehpura, Vadodara. The physicochemical properties of groundwater sample were determined and are tabulated in Table 6. A spike of standard fluoride solution (5–100 mg/L) was added to the groundwater and adsorption experiment was carried out with 0.2 g of adsorbent, at pH 1 with 3 h of contact time.

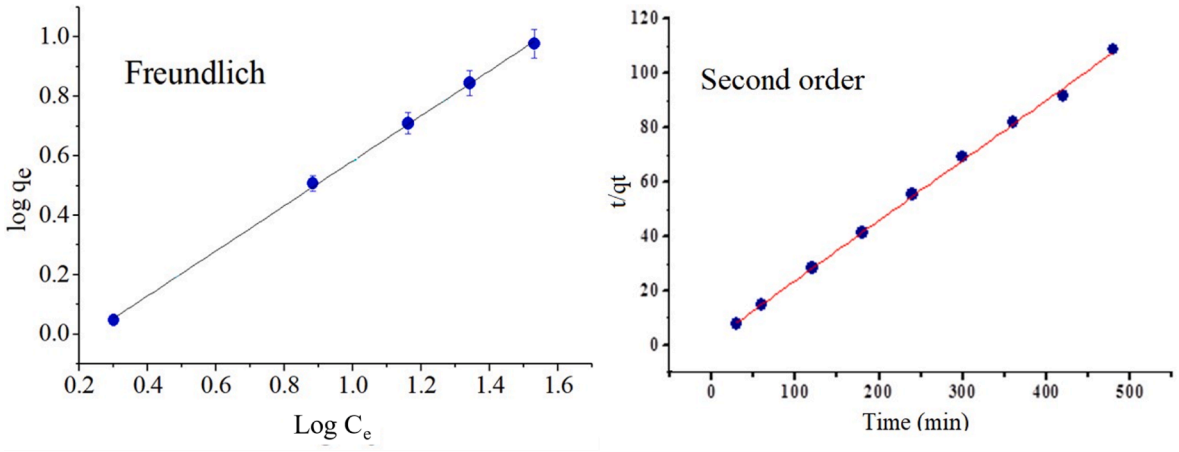

Fig. 5. Linear graph of Langumir isotherm and second order kinetics.

Table 3
Comparison of Adsorption Capacities of various literature reported adsorbents for fluoride with WMRBC.

Adsorbent	pH	q_{max}(mg/g)	Ref.
Waste carbon slurry	7.58	4.15	62
Banana peel	6	17.4	63
Groundnut shell	7	1.15	64
Sweet lemon peel	2–12	59.59	65
Agricultural waste	6	6	66
Mushroom compost biochar coated with aluminum hydroxide	6–8	36.5	67
Distiller's grains biochars coated by aluminum hydroxide	5–9	18.05	68
Activated Biochar of Colocasiaesculenta Stem	4.25	7.3	47
Steam-Activated Biochar Derived from Cocosnucifera Shell	6.5	0.95	69
Corn stover biochar	2	5.0	25
Magnetic corn stover biochar	2	3.41	25
Pine wood biochar	2	7.66	32
Pine Bark biochar	2	9.77	54
Hydrous manganese oxide-coated alum	4–6	7.09	70
WMRBC	1	9.5	This study

Table 4
Kinetic parameters of Pseudo first order, Pseudo Second Order, Intraparticle diffusion and Elovich models for the adsorption of fluoride onto WMRBC.

q_e(exp): 4.675 mg/g	q_e	K	r^2	A	B
Pseudo First order	0.7719	0.0032	0.7977		
Pseudo Second order	4.5269	1.7916	0.9997		
Intraparticle diffusion	10.5979	0.0216	0.9315		
Elovich	5.0676		0.9164	46100.35	4.0634

Table 5
Thermodynamic Parameters of fluoride adsorption onto WMRBC.

Thermodynamic parameter	Value
ΔG	–22.28 kJ/mole
ΔS	0.039 KJ mol^{-1} K^{-1}
ΔH	−10.46 KJ

It may be observed from Table S2 that fluoride could be effectively removed from both 5 and 10 mg/L spiked groundwater samples. The removal of fluoride by WMRBC could be by adsorption and electrostatic interactions while at higher concentrations precipitation on minerals might also be taking place [68]. Further, increase in initial fluoride concentration, may also have provided the necessary driving force to overcome the resistance to the mass transfer of fluoride to WMRBC and enhanced the interaction between fluoride and WMRBC.

3.2.9. *Application to industrial effluent sample*

The application of the synthesized adsorbent has been carried out with an untreated industrial effluent collected from a fluorochemical industry. The physicochemical parameters of the effluent are tabulated in Table 6.

The adsorption of fluoride on WMRBC in industrial effluent (25 mL) was carried out at pH 1, with dose of 0.2 g and 3 h contact time at ambient temperature. The fluoride concentration could be reduced to 2320 mg/L with ~ 56.7% adsorption and increased to 70% when the dose of WMRBC was increased to 1 g. The removal was appreciable in the presence of high concentrations of sulphate and chloride. The removal could further be improved by increasing the adsorbent dose and by multiple batch adsorption steps.

3.2.10. *Reuse of adsorbent*

Three consecutive adsorption–desorption cycles were performed to study desorption and regeneration of WMRBC. Desorption was observed to be 77.11% using 0.1 M NaOH solution. The % uptake of fluoride was found to be 79.54%, 71.99%, and 60.17% for the 1^{st} 2^{nd} and 3^{rd} cycle of batch operations respectively (Fig. 6b). The results indicated the usefulness and sustainability of adsorbent for commercial or industrial purposes.

4. Discussion

The adsorption capacity of WMRBC for fluoride was not consistent with its surface area (0.5365 m^2/g). This indicated that, multiple mechanisms must be operating in the adsorption process. The possible mechanisms have been proposed below:

a) The low heat of adsorption obtained from Temkin isotherm model (0.1016 J/mol) indicated that the adsorption process is physical in nature. Physical adsorption may occur primarily via Van der Waals forces [61].
b) XRD and EDS results revealed the presence of metals such as Mg, Ca, Si and K in the biochar which can form bonds with fluoride resulting in insoluble fluoride formation on the adsorbent.
c) The internal and outer surfaces of the biochar were reported to contain a rich variety of oxygen-containing functional groups including hydroxy, anhydride, carboxylic acid, ketone, quinone, ether, lactone, pyrone, catechol, hydroxy ketone, and others which are amenable for protonation and binding electrostatically with fluoride [33].
d) The possibility of ion exchange mechanism with anions associated with quaternary ammonium groups if any, has been reported for

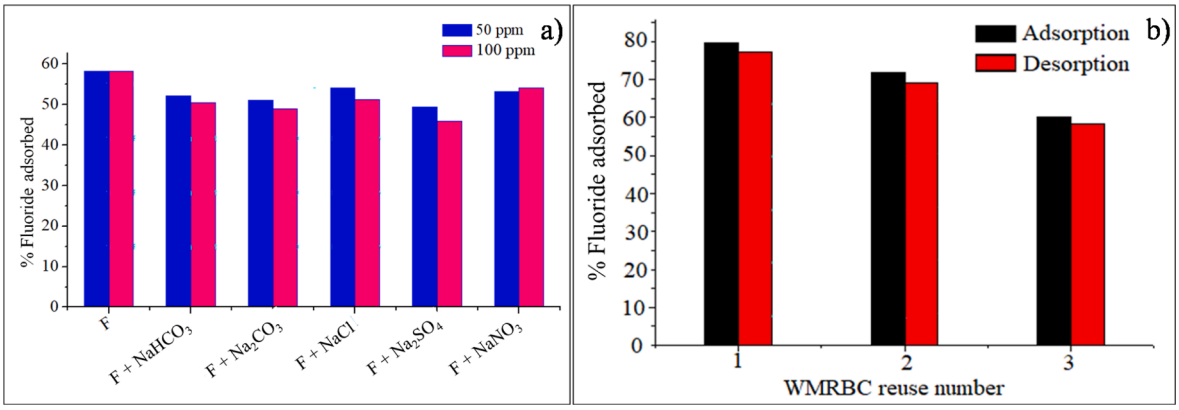

Fig. 6. a) Effect of competing anion concentration on % uptake of fluoride, b) Uptake of fluoride after consecutive 1st 2nd and 3rd cycle using 0.1 N NaOH as regenerant (Initial dose: 200 mg, pH 1, initial fluoride concentration: 50 mg/L).

Table 6
Characteristics of ground water and Industrial waste water.

SI.No.	Parameter	Value	
		Groundwater	Industrial effluent
1	pH	7.9	9.8
2	Conductivity μS/cm	7340	25,800
3	TDS mg/L	3670	129,000
4	Alkalinity mg/L	60	2600
5	Hardness mg/L	260	–
6	COD mg/L	16	12,160
7	Nitrate mg/L	620	–
8	Nitrite mg/L	42.9	–
9	Sulfate mg/L	161	154.0
10	Chloride mg/L	1497	6035
11	Fluoride mg/L	1.49	5570

removal of fluoride by Kumar et al. [4]. However, in the present work EDAX studies have shown the presence of chloride on both WMRBC and WMRBCF suggesting that ion exchange did not occur. TGA and IR studies have indicated the presence of dehydrated hemicellulose and cellulose residues which can result in an electrophilic carbon on the surface of biochar that can interact with fluoride ions [4].

The fluoride removal was thus attributed to a combination of electrostatic attraction and metal fluoride precipitation.

5. Conclusion

In this study biochar derived from watermelon rind, WMRBC was characterised and was successfully used for defluoridation of ground water and industrial effluents. Batch experiments indicated the optimum adsorption conditions of pH and contact time to be 1 and 3 h respectively. The adsorption data exhibited a better fit to the Freundlich isotherm model and followed pseudo second order kinetics. The negative values of free energy and enthalpy indicated the spontaneous and exothermic nature of the adsorption process. The maximum adsorption capacity of WMRBC for fluoride was 9.5 mg/g at pH 1.

However, the treated groundwater would need further treatment to adjust pH, which would require addition of Na_2CO_3/ $MgCO_3$/ $CaCO_3$ to increase pH. Modification of WMRBC to make it more amenable for removal of fluoride at neutral pH would be a part of our future studies. WMRBC is more feasible for treating industrial wastewater with low pH such as metal plating, soldering, glass manufacturing, phosphate fertilizer and semiconductor industries Common co-existing anions such as Cl^-, NO_3^-, SO_4^{2-}, $HCO_3^-$and CO_3^{2-} did not affect the fluoride adsorption potential of WMRBC. Furthermore, WMRBC retained ~ 60% of its adsorption capacity after being reused three times.

CRediT authorship contribution statement

Mohini Sadhu: Data curation, Formal analysis. **Prosun Bhattacharya:** Supervision, Validation, Visualization. **Meththika. Vithanage:** Supervision, Validation. **Pamidimukkala. Padmaja Sudhakar:** Conceptualization, Funding acquisition, Investigation, Methodology, Project administration, Supervision, Validation, Visualization.

Declaration of Competing Interest

The authors declare that they have no known competing financial interests or personal relationships that could have appeared to influence the work reported in this paper.

Acknowledgement

One of the authors Mohini Sadhu, would like to acknowledge DST WTI, New Delhi for financial assistance and Department of Chemistry, The Maharaja Sayajirao University of Baroda for laboratory facilities and DST FIST for BET facility. The authors would like to thank the reviewers for their valuable suggestions and comments during the review process. PB would like to acknowledge the Swedish International Development Cooperation Agency for the projects “Aquatic Pollution and Remediation in the Titicaca, Uru, Poopo High Altitude Lakes System” in Bolivia (Sida Contribution 75000553) and “Development of affordable adsorbent systems for arsenic and fluoride removal in the drinking water sources in Tanzania (DAFWAT) (Sida Contribution 51170072).

Appendix A. Supplementary material

Supplementary data to this article can be found online at https://doi.org/10.1016/j.seppur.2021.119106.

References

[1] P. Bhattacharya, J. Bundschuh, Groundwater for sustainable development - cross cutting the UN sustainable development goals - editorial, Groundw. Sustain. Dev. 1 (2015) 155–157, https://doi.org/10.1016/j.gsd.2016.04.004.
[2] J.P. Maity, M. Vithanage, M. Kumar, A. Ghosh, D. Mohan, A. Ahmad, P. Bhattacharya, Seven 21st century challenges of arsenic-fluoride contamination and remediation, Groundw. Sustain. Dev. 12 (2021), https://doi.org/10.1016/j.gsd.2020.100538.
[3] M. Vithanage, P. Bhattacharya, Fluoride in Drinking Water: Health Effects and Remediation, (2015) 105-151. https://doi.org/10.1007/978-3-319-11906-94.
[4] H. Kumar, M. Patel, D. Mohan, Simplified Batch and Fixed-Bed Design System for Efficient and Sustainable Fluoride Removal from Water Using Slow Pyrolyzed Okra

Stem and Black Gram Straw Biochars, ACS Omega 4 (2019) 19513–19525, https://doi.org/10.1021/acsomega.9b00877.
[5] J. Ijumulana, F. Ligate, P. Bhattacharya, F. Mtalo, C. Zhang, Spatial analysis and GIS mapping of regional hotspots and potential health risk of fluoride concentrations in groundwater of northern Tanzania, Sci. Total Environ. 735 (2020), 139584, https://doi.org/10.1016/j.scitotenv.2020.139584.
[6] J. Bundschuh, J.P. Maity, S. Mushtaq, M. Vithanage, S. Seneweera, J. Schneider, P. Bhattacharya, N.I. Khan, I. Hamawand, L.R.G. Guilherme, K. Reardon-Smith, F. Parvez, N. Morales-Simfors, S. Ghaze, C. Pudmenzky, L. Kouadio, C.Y. Chen, Medical geology in the framework of the sustainable development goals, Sci. Total Environ. 581–582 (2017) 87–104, https://doi.org/10.1016/j.scitotenv.2016.11.208.
[7] V. Kimambo, P. Bhattacharya, F. Mtalo, J. Mtamba, A. Ahmad, Fluoride occurrence in groundwater systems at global scale and status of defluoridation – State of the art, Groundw. Sustain. Dev. 9 (2019), 100223, https://doi.org/10.1016/j.gsd.2019.100223.
[8] S. Ali, Y. Fakhri, M. Golbini, S.K. Thakur, A. Alinejad, I. Parseh, S. Shekhar, P. Bhattacharya, Concentration of fluoride in groundwater of India: A systematic review, meta-analysis and risk assessment, Groundw. Sustain. Dev. 9 (2019), 100224, https://doi.org/10.1016/j.gsd.2019.100224.
[9] J. Zhu, H. Zhao, J. Ni, Fluoride distribution in electrocoagulation defluoridation process, Sep. Purif. Technol. 56 (2007) 184–191, https://doi.org/10.1016/j.seppur.2007.01.030.
[10] J. Ijumulana, F. Ligate, R. Irunde, P. Bhattacharya, J.P. Maity, A. Ahmad, F. Mtalo, Spatial uncertainties in fluoride levels and health risks in endemic fluorotic regions of northern Tanzania, Groundw. Sust. Dev. (2021), 100618, https://doi.org/10.1016/j.gsd.2021.100618. In press.
[11] G. Jacks, P. Bhattacharya, V. Chaudhary, K.P. Singh, Controls on the genesis of some high-fluoride groundwaters in India, Appl. Geochemistry. 20 (2005) 221–228, https://doi.org/10.1016/j.apgeochem.2004.07.002.
[12] N. Mameri, A.R. Yeddou, H. Lounici, D. Belhocine, H. Grib, B. Bariou, Defluoridation of septentrional Sahara water of north Africa by electrocoagulation process using bipolar aluminium electrodes, Water Res. 32 (1998) 1604–1612, https://doi.org/10.1016/S0043-1354(97)00357-6.
[13] N. Kabay, H. Kodama, Ion exchange properties of $BiO(NO_3)\cdot 0.5H_2O$ towards fluoride ions, Solvent Extr. Ion Exch. 18 (2000) 583–603, https://doi.org/10.1080/07366290008934699.
[14] K.M. Popat, P.S. Anand, B.D. Dasare, Selective removal of fluoride ions from water by the aluminium form of the aminomethylphosphonic acid-type ion exchanger, React. Polym. 23 (1994) 23–32, https://doi.org/10.1016/0923-1137(94)90107-4.
[15] C.L. Yang, R. Dluhy, Electrochemical generation of aluminum sorbent for fluoride adsorption, J. Hazard. Mater. 94 (2002) 239–252, https://doi.org/10.1016/S0304-3894(02)00066-3.
[16] H. Paudyal, B. Pangeni, K. Inoue, H. Kawakita, K. Ohto, H. Harada, S. Alam, Adsorptive removal of fluoride from aqueous solution using orange waste loaded with multi-valent metal ions, J. Hazard. Mater. 192 (2011) 676–682, https://doi.org/10.1016/j.jhazmat.2011.05.070.
[17] P.I. Ndiaye, P. Moulin, L. Dominguez, J.C. Millet, F. Charbit, Removal of fluoride from electronic industrial effluentby RO membrane separation, Desalination 173 (2005) 25–32, https://doi.org/10.1016/j.desal.2004.07.042.
[18] J. Shen, A. Schäfer, Removal of fluoride and uranium by nanofiltration and reverse osmosis: A review, Chemosphere 117 (2014) 679–691, https://doi.org/10.1016/j.chemosphere.2014.09.090.
[19] E. Kir, E. Alkan, Fluoride removal by Donnan dialysis with plasma-modified and unmodified anion-exchange membranes, Desalination 197 (2006) 217–224, https://doi.org/10.1016/j.desal.2006.01.018.
[20] V. Khatibikamal, A. Torabian, F. Janpoor, G. Hoshyaripour, Fluoride removal from industrial wastewater using electrocoagulation and its adsorption kinetics, J. Hazard. Mater. 179 (2010) 276–280, https://doi.org/10.1016/j.jhazmat.2010.02.089.
[21] J. Ge, J. Qu, P. Lei, H. Liu, New bipolar electrocoagulation-electroflotation process for the treatment of laundry wastewater, Sep. Purif. Technol. 36 (2004) 33–39, https://doi.org/10.1016/S1383-5866(03)00150-3.
[22] A. Bhatnagar, E. Kumar, M. Sillanpää, Fluoride removal from water by adsorption-A review, Chem. Eng. J. 171 (2011) 811–840, https://doi.org/10.1016/j.cej.2011.05.028.
[23] A. Bhatnagar, E. Kumar, M. Sillanpää, Fluoride removal from water by adsorption — A review, Chem. Eng. J. 171 (2011) 811–840, https://doi.org/10.1016/j.cej.2011.05.028.
[24] N. Bordoloi, R. Goswami, M. Kumar, R. Kataki, Biosorption of Co (II) from aqueous solution using algal biochar: Kinetics and isotherm studies, Bioresour. Technol. 244 (2017) 1465–1469, https://doi.org/10.1016/j.biortech.2017.05.139.
[25] M. Ahmad, A.U. Rajapaksha, J.E. Lim, M. Zhang, N. Bolan, D. Mohan, M. Vithanage, S.S. Lee, Y.S. Ok, Biochar as a sorbent for contaminant management in soil and water: A review, Chemosphere 99 (2014) 19–33, https://doi.org/10.1016/j.chemosphere.2013.10.071.
[26] D. Mohan, S. Kumar, A. Srivastava, Fluoride removal from ground water using magnetic and nonmagnetic corn stover biochars, Ecol. Eng. 73 (2014) 798–808, https://doi.org/10.1016/j.ecoleng.2014.08.017.
[27] C.E. Brewer, K. Schmidt-Rohr, J.A. Satrio, R.C. Brown, Characterization of biochar from fast pyrolysis and gasification systems, Environ. Prog. Sustain. Energy. 28 (2009) 386–396, https://doi.org/10.1002/ep.10378.
[28] S. Kloss, F. Zehetner, A. Dellantonio, R. Hamid, F. Ottner, V. Liedtke, M. Schwanninger, M.H. Gerzabek, G. Soja, Characterization of slow pyrolysis biochars: effects of feedstocks and pyrolysis temperature on biochar properties, J. Environ. Qual. 41 (2011) 990–1000, https://doi.org/10.2134/jeq2011.0070.
[29] A.C. Mesa, K.A. Spokas, Impacts of biochar (Black Carbon) additions on the sorption and efficacy of herbicides, Herbic. Environ. (2011) 315–340.
[30] H. Wang, K. Lin, Z. Hou, B. Richardson, J. Gan, Sorption of the herbicide terbuthylazine in two New Zealand forest soils amended with biosolids and biochars, J. Soils Sediments. 10 (2010) 283–289, https://doi.org/10.1007/s11368-009-0111-z.
[31] X.B. Yang, G.G. Ying, P.A. Peng, L. Wang, J.L. Zhao, L.J. Zhang, P. Yuan, H.P. He, Influence of biochars on plant uptake and dissipation of two pesticides in an agricultural soil, J. Agric. Food Chem. 58 (2010) 7915–7921, https://doi.org/10.1021/jf1011352.
[32] M. García-Jaramillo, L. Cox, H.E. Knicker, J. Cornejo, K.A. Spokas, M.C. Hermosín, Characterization and selection of biochar for an efficient retention of tricyclazole in a flooded alluvial paddy soil, J. Hazard. Mater. 286 (2015) 581–588, https://doi.org/10.1016/j.jhazmat.2014.10.052.
[33] N. Gandhi, D. Sirisha, K.B. Chandra Sekhar, A. Smitha, Removal of fluoride from water and waste water by using low cost adsorbents, Int. J. PharmTech Res. 4 (2012) 1646–1653.
[34] M.P. Tarazona-Díaz, J. Viegas, M. Moldao-Martins, E. Aguayo, Bioactive compounds from flesh and by-product of fresh-cut watermelon cultivars, J. Sci. Food Agric. 91 (2011) 805–812, https://doi.org/10.1002/jsfa.4250.
[35] C. Petkowicz, L. Vriesmann, P.A. Williams, Pectins from food waste: Extraction, characterization and properties of watermelon rind pectin, Food Hydrocoll. 65 (2016) 57–67, https://doi.org/10.1016/j.foodhyd.2016.10.040.
[36] X. Jin, F. Xi, D. Lv, Q. Wu, X. Lin, The effect of the chitosan membrane properties on the enzyme adsorption and performance for the construction of horseradish peroxidase biosensors, Carbohydr. Polym. 85 (2011) 786–791, https://doi.org/10.1016/j.carbpol.2011.03.048.
[37] P. Budrat, A. Shotipruk, Enhanced recovery of phenolic compounds from bitter melon (Momordica charantia) by subcritical water extraction, Sep. Purif. Technol. 66 (2009) 125–129, https://doi.org/10.1016/j.seppur.2008.11.014.
[38] R. Horax, N. Hettiarachchy, S. Islam, Total Phenolic Contents and Phenolic Acid Constituents in 4 Varieties of Bitter Melons (Momordica charantia) and Antioxidant Activities of Their Extracts, J. Food Sci. 70 (2005) 275–280, https://doi.org/10.1111/j.1365-2621.2005.tb07173.x.
[39] M. Keiluweit, P.S. Nico, M. Johnson, M. Kleber, Dynamic molecular structure of plant biomass-derived black carbon (biochar), Environ. Sci. Technol. 44 (2010) 1247–1253, https://doi.org/10.1021/es9031419.
[40] Z.Q. Li, C.J. Lu, Z.P. Xia, Y. Zhou, Z. Luo, X-ray diffraction patterns of graphite and turbostratic carbon, Carbon N. Y. 45 (2007) 1986–11695, https://doi.org/10.1016/j.carbon.2007.03.038.
[41] W. Wu, M. Yang, Q. Feng, K. McGrouther, H. Wang, H. Lu, Y. Chen, Chemical characterization of rice straw-derived biochar for soil amendment, Biomass Bioenergy 47 (2012) 268–276, https://doi.org/10.1016/j.biombioe.2012.09.034.
[42] B. Dari, V.D. Nair, W.G. Harris, P.K.R. Nair, L. Sollenberger, R. Mylavarapu, Relative influence of soil- vs. biochar properties on soil phosphorus retention, Geoderma 280 (2016) 82–87, https://doi.org/10.1016/j.geoderma.2016.06.018.
[43] A. Cabeza, F. Sobrón, F.M. Yedro, J. García-Serna, Autocatalytic kinetic model for thermogravimetric analysis and composition estimation of biomass and polymeric fractions, Fuel 148 (2015) 212–225, https://doi.org/10.1016/j.fuel.2015.01.048.
[44] S.H. Dhawane, A.A. Khan, K. Singh, A. Tripathi, R. Hasda, G. Halder, Insight into Optimization, isotherm, kinetics, and thermodynamics of fluoride adsorption onto activated alumina, Environ. Prog. Sustain. Energy. 37 (2017) 766–776, https://doi.org/10.1002/ep.12814.
[45] S. Mukherjee, G. Halder, Assessment of fluoride uptake performance of raw biomass and activated biochar of Colocasia esculenta stem: Optimization through response surface methodology, Environ. Prog. Sustain. Energy. 35 (2016) 1305–1316, https://doi.org/10.1002/ep.12346.
[46] T. Mimmo, P. Panzacchi, M. Baratieri, C.A. Davies, G. Tonon, Effect of pyrolysis temperature on miscanthus (Miscanthus × giganteus) biochar physical, chemical and functional properties, Biomass Bioenergy 62 (2014) 149–157, https://doi.org/10.1016/j.biombioe.2014.01.004.
[47] D. Chen, X. Yu, C. Song, X. Pang, J. Huang, Y. Li, Effect of pyrolysis temperature on the chemical oxidation stability of bamboo biochar, Bioresour. Technol. 218 (2016) 1303–1306, https://doi.org/10.1016/j.biortech.2016.07.112.
[48] M. Kishore, Preparation and development of adsorbent carbon from acacia farnesiana for defluoridation, Int. J. Plant, Animal Environ. Sci. 1 (3) (2011) 209–223.
[49] M. Schwanninger, J.C. Rodrigues, H. Pereira, B. Hinterstoisser, Effects of short-time vibratory ball milling on the shape of FT-IR spectra of wood and cellulose, Vib. Spectrosc. 36 (2004) 23–40, https://doi.org/10.1016/j.vibspec.2004.02.003.
[50] R.K. Sharma, J.B. Wooten, V.L. Baliga, X. Lin, W.G. Chan, M.R. Hajaligol, Characterization of chars from pyrolysis of lignin, Fuel 83 (2004) 1469–1482, https://doi.org/10.1016/j.fuel.2003.11.015.
[51] S. Kushwaha, G. Sreelatha, P. Padmaja, Physical and chemical modified forms of palm shell: Preparation, characterization and preliminary assessment as adsorbents, J. Porous Mater. 20 (2013) 21–36, https://doi.org/10.1007/s10934-012-9571-4.
[52] ASTM International, Standard Test Method for Determination of Iodine Number of Activated Carbon, ASTM Stand. 15 (2004) 1–5, https://doi.org/10.1520/D4607-14.2.
[53] D. Mohan, R. Sharma, V.K. Singh, P. Steele, C.U. Pittman, Fluoride Removal from Water using Bio-Char, a Green Waste, Low-Cost Adsorbent: Equilibrium Uptake and Sorption Dynamics Modeling, Ind. Eng. Chem. Res. 51 (2012) 900–914, https://doi.org/10.1021/ie202189v.
[54] D.A.P. Tanaka, S. Kerketta, M.A.L. Tanco, T. Yokoyama, T.M. Suzuki, Adsorption of fluoride ion on the zirconium(IV) complexes of the chelating resins functionalized

with amine-N-acetate ligands, Sep. Sci. Technol. 37 (2002) 877–894, https://doi.org/10.1081/SS-120002221.
[55] J. Zhou, Y. Liu, Y. Han, F. Jing, J. Chen, Bone-derived biochar and magnetic biochar for effective removal of fluoride in groundwater: Effects of synthesis method and coexisting chromium, Water Environ. Res. 91 (2019) 588–597, https://doi.org/10.1002/wer.1068.
[56] G. Patel, U. Pal, S. Menon, Removal of Fluoride from Aqueous Solution by CaO Nanoparticles, Sep. Sci. Technol. 44 (2009) 2806–2826, https://doi.org/10.1080/01496390903014425.
[57] M.G. Sujana, S. Anand, Fluoride removal studies from contaminated ground water by using bauxite, Desalination 267 (2011) 222–227, https://doi.org/10.1016/j.desal.2010.09.030.
[58] Z. Jin, X. Wang, Y. Sun, Y. Ai, X. Wang, Adsorption of 4-n-Nonylphenol and Bisphenol-A on Magnetic Reduced Graphene Oxides: A Combined Experimental and Theoretical Studies, Environ. Sci. Technol. 49 (2015) 9168–9175, https://doi.org/10.1021/acs.est.5b02022.
[59] H.M.F. Freundlich, Uber die adsorption in lasungen, J. Phys. Chem. 57 (1906) 385–470.
[60] M.J. Temkin, V. Pyzhev, Recent modifications to Langmuir isotherms, Acta Physico-chimica USSR. 12 (1940) 217–222, https://doi.org/10.1016/j.jhazmat.2008.12.093.
[61] C.A. Başar, Applicability of the various adsorption models of three dyes adsorption onto activated carbon prepared waste apricot, J. Hazard. Mater. 135 (2006) 232–241, https://doi.org/10.1016/j.jhazmat.2005.11.055.
[62] D. Rehrah, M.R. Reddy, J.M. Novak, R.R. Bansode, K.A. Schimmel, J. Yu, D. W. Watts, M. Ahmedna, Production and characterization of biochars from agricultural by-products for use in soil quality enhancement, J. Anal. Appl. Pyrolysis. 108 (2014) 301–309, https://doi.org/10.1016/j.jaap.2014.03.008.
[63] Y. Lee, P.R.B. Eum, C. Ryu, Y.K. Park, J.H. Jung, S. Hyun, Characteristics of biochar produced from slow pyrolysis of Geodae-Uksae 1, Bioresour. Technol. 130 (2013) 345–350, https://doi.org/10.1016/j.biortech.2012.12.012.
[64] R. Borah, D. Kumari, A. Gogoi, S. Biswas, R. Goswami, J. Shim, N.A. Begum, M. Kumar, Efficacy and field applicability of Burmese grape leaf extract (BGLE) for cadmium removal: An implication of metal removal from natural water, Ecotoxicol. Environ. Saf. 147 (2018) 585–593, https://doi.org/10.1016/j.ecoenv.2017.09.002.
[65] Y.S. Ho, G. McKay, Sorption of dye from aqueous solution by peat, Chem. Eng. J. 70 (1998) 115–124, https://doi.org/10.1016/S1385-8947(98)00076-X.
[66] T.A. Khan, S.A. Chaudhry, I. Ali, Equilibrium uptake, isotherm and kinetic studies of Cd(II) adsorption onto iron oxide activated red mud from aqueous solution, J. Mol. Liq. 202 (2015) 165–175, https://doi.org/10.1016/j.molliq.2014.12.021.
[67] Ö. Gerçel, A. Özcan, A.S. Özcan, H.F. Gerçel, Preparation of activated carbon from a renewable bio-plant of Euphorbia rigida by H_2SO_4 activation and its adsorption behavior in aqueous solutions, Appl. Surf. Sci. 253 (2007) 4843–4852, https://doi.org/10.1016/j.apsusc.2006.10.053.
[68] S. Budyanto, Y.-L. Kuo, J.C. Liu, Adsorption and precipitation of fluoride on calcite nanoparticles: A spectroscopic study, Sep. Purif. Technol. 150 (2015) 325–331, https://doi.org/10.1016/j.seppur.2015.07.016.